Catal Lett (2008) 122:57–67
DOI 10.1007/s10562-007-9351-y

SBA-15 as Support for MoS_2 and Co-MoS_2 Catalysts Derived from Thiomolybdate Complexes in the Reaction of HDS of DBT

Z.-D. Huang · W. Bensch · L. Kienle · S. Fuentes · G. Alonso · C. Ornelas

Received: 11 September 2007 / Accepted: 8 November 2007 / Published online: 27 November 2007

Abstract Molybdenum sulfide and cobalt-molybdenum sulfide catalysts supported on mesoporous SBA-15 were prepared by thermal decomposition of ammonium thiomolybdate (ATM). SBA-15 was synthesized at 353 K and 413 K to obtain pore diameters of about 6 and 9 nm, respectively. The (Co)-MoS_2/SBA-15 catalysts were characterized with X-ray diffraction (XRD), N_2-physisorption and high-resolution transmission electron microscopy (HRTEM). HRTEM images give evidence for the presence of a poorly dispersed MoS_2 phase with long MoS_2 slabs and a pronounced MoS_2 stacking. The catalytic performance in the hydrodesulfurization (HDS) reaction of dibenzothiophene (DBT) was examined at $T = 623$ K and $P = 3.4$ MPa. The Co-MoS_2/SBA-15 materials show a relatively high catalytic activity with a strong preference for the direct desulfurization (DDS) pathway. This is an interesting result in view of the significant stacking of MoS_2 particles and the size of the slabs. The generation of the catalytically active CoMoS phase and a large number of coordinately unsaturated sites (CUS) may explain the high performance of Co promoted MoS_2/SBA-15 catalysts in the HDS reaction. A confinement effect of the mesoporous channels of SBA-15 is observed for the unpromoted MoS_2/SBA-15 catalysts. SBA-15 with 9 nm channel diameter with 11 wt.% Mo loading shows a higher selectivity for the hydrogenation pathway than SBA-15 with 6 nm channel and 16 wt.% Mo loading.

Keywords Hydrodesulfurization · Ammonium thiomolybdate · Co-MoS_2/SBA-15 catalysts · HRTEM · Coordinately unsaturated sites (CUS) · SBA-15 support

Z.-D. Huang · W. Bensch (✉)
Institut für Anorganische Chemie, University of Kiel, Olshausenstraße 40-60, 24098 Kiel, Germany
e-mail: wbensch@ac.uni-kiel.de

L. Kienle
Max-Planck-Institut für Festkörperforschung, Heisenbergstr. 1, 70506 Stuttgart, Germany

S. Fuentes
Centro de Ciencias de la Materia Condensada, UNAM, Ensenada, Baja California C.P. 22860, Mexico

G. Alonso · C. Ornelas
Centro de Investigación en Materiales Avanzados S. C., Chihuahua, Chih. C.P. 31109, Mexico

1 Introduction

More stringent limitations to sulfur contents of transportation fuels lead to continuing quest for better performing hydrodesulfurization (HDS) catalysts. One of the successful ways to improve the catalyst activity is to synthesize transition metal sulfides on a porous support material which can well control the structure of the catalyst. Most commercially available HDS catalysts are supported on alumina with a surface area of about 200 m^2/g. Mesoporous silica materials such as MCM-41 [1, 2] and SBA-15 [3] with their well ordered hexagonal pore structures, narrow pore diameters (3–30 nm) and higher surface areas (more than 700 m^2/g) offer several advantages in comparison with alumina. MCM-41 supported Co(Ni)Mo catalysts were investigated in the last decade [4–7]. The catalysts exhibited higher activities for conversion of dibenzothiophene (DBT) and petroleum residues than Co(Ni)-Mo/γ-Al_2O_3 at high molybdenum loading [4] or high atomic ratio Co(Ni)-Mo [5, 6]. More recently, mesoporous SBA-15 has been in the focus of research interests due to the larger pores, thicker pore walls and higher hydrothermal stability compared to MCM-41. Indeed, Vradman et al. [8, 9]

demonstrated the excellent potential of high loading Ni-W/SBA-15 catalysts for deep hydrotreatment of petroleum feedstocks. The catalysts prepared by an ultrasonication route showed a high HDS activity. Mesoporous SBA-15 was also found to be a suitable support for Mo, CoMo, and NiMo catalysts as reported by Rao and co-workers [10]. Furthermore, Al, Ti and Zr containing SBA-15 supported NiMo or CoMo catalysts were prepared by Klimova and co-workers [11, 12], Rao and co-workers [13] and Fierro and co-workers [14]. They observed that SBA-15 modified with these hetero-atoms (Al, Ti, Zr) provides better dispersion for the deposited Ni(Co) and Mo active species and yields considerably high activity for HDS of DBT.

In the majority cases these hydrotreating catalysts were prepared via an oxide route, i.e. the MCM-41 or SBA-15 materials containing transition metal salts like ammonium heptamolybdate, nickel (cobalt) nitrate or nickel (cobalt) acetate were calcined to produce stable oxides. The oxides must then be sulfided either prior to or during the start-up of the hydrotreatment process in a stream of H_2S (15%) in H_2. Catalysts processed with such a procedure exhibit HDS activity being strongly influenced by the calcination temperature, the temperature and pressure for transformation to the sulfide [15]. On the other hand, molybdenum and tungsten sulfide catalysts for hydrotreating reactions can be obtained directly by decomposition of the corresponding thiometallates. It was observed that the thermal decomposition of molybdenum and tungsten thiosalts is an effective method for the production of improved unsupported catalysts. One reason is that no metal-sulfur bond formation is required which is necessary applying the oxide route [16–19]. However, to the best of our knowledge only a few studies have been performed to investigate supported MoS_2 catalysts derived from ammonium thiomolybdate (ATM) as precursor [20, 21].

The aim of this work was to study the SBA-15 support with different pore sizes (6 nm and 9 nm) for MoS_2 and MoS_2 promoted with Co catalysts using ATM as molybdenum source in the HDS of DBT reaction. The supported catalysts were characterized with X-ray diffractometry (XRD), nitrogen physisorption using the Brunauer, Emmett and Teller (BET) method and high-resolution transmission electron microscopy (HRTEM).

2 Experimental

2.1 Sample Preparation

2.1.1 Synthesis of Pristine Mesoporous SBA-15 [22–24]

Eight gram of poly(ethyleneglycol)-block-poly(propyleneglycol)-block-poly(ethyleneglycol) triblock copolymer (Aldrich, pluronic, P-123) was dissolved in 240 g of water and 28.6 g of concentrated hydrochloric acid at 303 K on a water bath. After drop wise addition of 16 g of tetraethylorthosilicate (TEOS), the reaction mixture was stirred for 24 h at 303 K. The resulting gel was transferred into a Teflon bottle and heated to 353 K and 413 K for 24 h to obtain SBA-15 with 6 nm and 9 nm pores, respectively. The resulting white powder was filtered and washed with deionized water, and the surfactant was removed by Soxleth extraction at 351 K with a mixture of 970 mL of ethanol and 30 mL of concentrated hydrochloric acid. After washing with ethanol, the white powder was dried at room temperature under vacuum for about one week.

2.1.2 Synthesis of MoS_2/SBA-15

Typically, 2 g of SBA-15 was stirred in aqueous solutions of ammonium thiomolybdate $(NH_4)_2MoS_4$ (ATM) with different concentrations. After stirring at room temperature for 20 h the products were filtered without washing. Materials containing different Mo concentrations were prepared using appropriate concentrations of ATM and the final products were stored in dry air. The synthesized samples are denoted as Mo(*X*)/SBA-15(*Y*) in the figure legends, where *X* is the Mo loading in wt.% and *Y* is the pore size of SBA-15.

2.1.3 Synthesis of Co-MoS_2/SBA-15

Supported Co-Mo catalysts were prepared by impregnation of SBA-15 with $Co(CH_3COO)_2{\cdot}4H_2O$ followed by evaporation of H_2O and CH_3COOH at 773 K for 3 h. At this temperature the pink $(CH_3COO)_2Co{\cdot}4H_2O$/SBA-15 material turned blue indicating the formation of Co silicates. Under H_2S atmosphere the blue Co/SBA-15 reacted easily to form CoS_x/SBA-15. It was stirred in aqueous solutions of ATM and then treated with the same procedure used for the synthesis of MoS_2/SBA-15 to prepare Co-Mo/SBA-15. The samples are named as Co(*X*)Mo(*Y*)/SBA-15(*Z*) in the figure legends, where *X* is the Co loading in wt.%, *Y* is the Mo loading in wt.%, and *Z* is the pore size of SBA-15.

2.2 Sample Characterization

X-ray diffraction (XRD) patterns were obtained on a Bruker D8 Advance diffractometer at room temperature using $CuK_{\alpha 1}$ radiation. Nitrogen adsorption measurements were carried out at 77 K on a Sorptomatic 1990 adsorption analyzer. Before the measurements, the samples were out gassed for at least 24 h at 393 K. The BET surface areas

were calculated from $p/p_0 = 0.03–0.3$ in the adsorption branch.

A prominent classical method used for the analysis of the pore size distributions (PSD) from sorption isotherms is the Barrett-Joyner-Halenda (BJH) approach, which is based on macroscopic thermodynamic models such as the modified Kelvin equation for cylindrical pores [25]. The evaluation of the PSD of mesoporous materials applying the BJH method is widely used in literature (see for example references [8, 10–12, 14, 22, 23]). Compared to other methods like the non-local density functional theory (NLDFT) the BJH analysis slightly underestimates the pore size of mesoporous materials [26, 27]. Nevertheless, the BJH method yields reasonable values for the PSD and changes of the pore size due to the presence of guest species in the channels are undoubtedly detected. In the present work the BJH method was applied for the calculation of the PSD using the desorption branch of the adsorption isotherms. HRTEM and SAED were performed with a Philips CM 30ST microscope (300 kV, LaB_6 cathode, C_S = 1.15 mm). A perforated carbon/copper net served as support for the particles of Co-Mo/SBA-15 (9 nm). SAED patterns were obtained using a diaphragm which limited the diffraction to a circular selected area (diameter: 250 nm). All images were recorded with a Gatan Multiscan CCD camera and evaluated (including Fourier analyses) with the program Digital Micrograph 3.6.1 (Gatan). EDX analyses were performed in the nanoprobe mode of CM30ST with a Si/Li detector (Noran, Vantage System). The Mo and Co contents of the different materials were determined by means of Inductively Coupled Plasma (ICP) analyses.

Prior to the catalytic test, the catalysts were activated at 500 K for 3 h under a H_2/N_2 (H_2, 10%) gas flow at atmospheric pressure. HDS of DBT was carried out in a Parr model 4522 high-pressure batch reactor. One gram of the catalyst and 150 mL of the freshly prepared solution of DBT in decaline (5% w/w $[DBT]_0 = 0.2388$ mol/L) was introduced in the reactor. The reactor was then purged and pressurized to 3.4 MPa (490 psi) with hydrogen and then heated up to 623 K at a rate change for with slope of 10 K/min and continuous stirring of 600 rpm. After reaching the working temperature, the products were collected for chromatographic analysis every half an hour to determine the conversion-time dependence during 5 h. After the reaction, the used catalysts were filtered, washed and stored in inert atmosphere. The reaction products were analyzed using a Perkin-Elmer Auto-system chromatograph with a 9 ft long × 1/8 inch diameter packed column containing chromosorb W-AW 80/100 mesh 3% OV-17 (phenyl methyl silicone 50% phenyl) as a separating phase. Estimated errors in the activity measurements are ±2%.

3 Results and Discussion

3.1 Powder XRD

In Fig. 1 the XRD patterns of MoS_2/SBA-15 and MoS_2/SBA-15 promoted with Co (6 nm and 9 nm) are displayed. An intense peak at about 1.0° 2θ and two distinct weak reflections between 1.5 and 2.0° 2θ are observed which are the characteristic reflections (100), (110), and (200) of

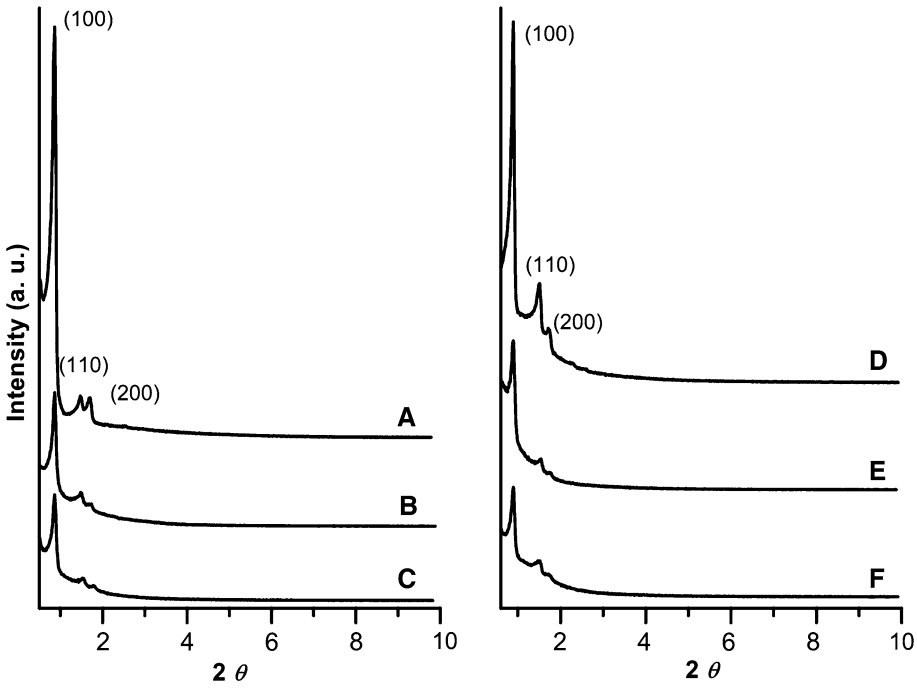

Fig. 1 XRD patterns of (A) SBA-15 (6 nm), (B) Mo(9)/SBA-15 (6 nm), (C) Co(2)Mo(10)/SBA-15 (6 nm), (D) SBA-15 (9 nm), (E) Mo(11)/SBA-15 (9 nm) and (F) Co(2)Mo(10)SBA-15 (9 nm)

hexagonal mesoporous SBA-15 with space group *p6mm*. The existence of these characteristic peaks evidences that the primary structure of the material consists of well ordered channels which are maintained after the Co and Mo incorporation. However, after loading of SBA-15 with MoS_2/Co-MoS_2 the intensity of the reflections decreased. This phenomenon is well known and is caused by the strong absorption of X-rays by Mo and/or a partial loss of the high order of the mesostructure [11].

Wide-angle XRD patterns of Co-Mo catalysts supported on SBA-15 with pore size of 6 nm are shown in Fig. 2. In addition to a broad modulation at about 22° 2θ caused by SBA-15, reflections at 14.4, 33, 40, and 58° 2θ correspond to the poorly crystalline structure of 2H-MoS_2 in all patterns. The asymmetric shape of the reflections at 33, 40, and 58° 2θ is a typical feature of layered materials with a partial turbostratic disorder. The average particle size of MoS_2 can be estimated from the peak width using the Scherrer formula, $d = 0.941\lambda/B\ \cos\theta_B$, where d is the mean diameter of the particle, λ is the wavelength of the Cu $K_{\alpha 1}$ line (0.154056 nm), θ_B is the angle between the incident beam and the reflecting lattice planes, and B is the width of the diffraction peak. The average crystallite size of MoS_2 estimated from the (002) reflection is typically about 4 nm (see Table 1), i.e., on average six layers of MoS_2 form the stacks in the c direction. The mean crystallite size of MoS_2 increases with increasing Mo loading for catalysts with the same Co content (Table 1). Comparing the sizes of MoS_2 nanoparticles with the pore diameters of the SBA-15 materials, a possible explanation is that the crystallites are located inside the channels of SBA-15 being directed along the channel axis. With increasing Co content up to ca. 3 wt.% an enlargement of the particle size of MoS_2 to about 6 nm is observed (Table 1, Fig. 2C). It suggests that the CoS_x particles inside the channels hinder the dispersion of ATM along the channels. In addition to the reflections of MoS_2, reflections of the stable Co_9S_8 phase appear at 30 and 52° 2θ. The peaks of Co_9S_8 are almost absent for high Mo-loading (Fig. 2B), which indicates the generation of an increasing amount of the catalytically active CoMoS phases.

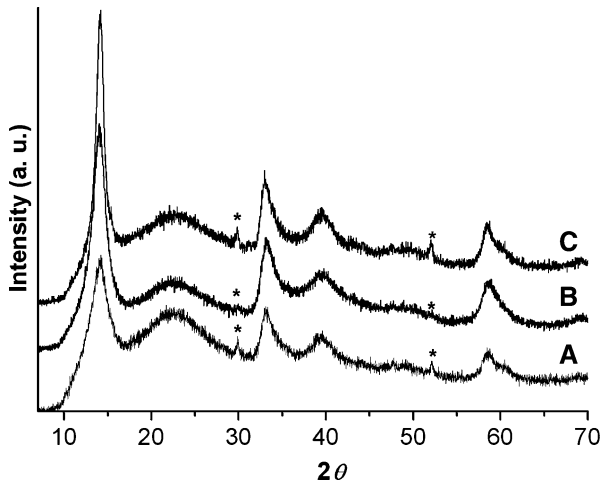

Fig. 2 Wide-angle XRD patterns of (A) Co(2)Mo(10)/SBA-15 (6 nm), (B) Co(2)Mo(20)/SBA-15 (6 nm); (C) Co(3)Mo(14)/ SBA-15 (6 nm). (*) Co_9S_8

3.2 Nitrogen Physisorption

In Figs. 3 and 4 the N_2 adsorption–desorption isotherms (at 77 K) and the pore-size distribution of SBA-15 and the impregnated SBA-15 materials with different metal loading are displayed. The amount of adsorbed nitrogen, which is associated with the specific surface area, is clearly larger for SBA-15 synthesized at 353 K in comparison with SBA-15 prepared at 413 K. The specific surface areas and pore volumes were determined by application of the BET equation and the numerical data are listed in Table 1. The capillary condensation step shows as a sharp increase of the adsorbed N_2 volume at a relative pressure $p/p_0 = 0.6$–0.8 with a hysteresis loop type H1 typically of mesoporus materials. The sharpness of this condensation step indicates the uniformity of mesopore sizes. The pore sizes were calculated from the desorption branch of the isotherms. For SBA-15 materials as well as the MoS_2/SBA-15 and Co-MoS_2/SBA-15 catalysts a type IV isotherm is observed, which is the typical feature for mesoporous materials [28], evidencing that the incorporation of Co and Mo species does not destroy the mesoporous structure of SBA-15. However, the nitrogen physisorption isotherm of impregnated SBA-15 materials displays some changes: (1) The mean pore diameter is shifted marginally towards higher values after introduction of Mo and Co in SBA-15, a phenomenon which was reported previously [13]; (2) The normalized surface area and pore volume decrease after the incorporation of metal sulfides (Table 1). This effect may be caused by partial pore blocking by the MoS_2/Co-MoS_2 phases, because the formation of Mo and Co sulfides inside the channels of the SBA-15 material should not significantly affect the pore volume due to their high density. Moreover, the normalized surfaces areas which are related to the pore blocking effects are higher for the Co-Mo_2/SBA-15 (9 nm) samples (>0.9) than for the catalysts supported on SBA-15 (6 nm) (0.55–0.70). The large pore diameter of 9 nm seems to be more suitable for the application as catalyst support because of the less pronounced pore blocking effects. It should be noted that the surface area of 9 nm SBA-15 (ca. 467 m^2/g) is obviously lower compared to the 6 nm SBA-15 (ca. 842 m^2/g, see Table 1).

Table 1 Specific surface area, normalized surface area, pore volume and normalized pore volume of SBA-15 support and Co-Mo sulfide catalysts supported on SBA-15 and the mean MoS_2 crystal size supported on SBA-15

Catalysts	Mo (wt.%)	Co (wt.%)	Pore volume ($cm^3\ g^{-1}$)		BET surface area ($m^2\ g^{-1}$)		MoS_2 mean crystal size (nm)
			Normalized		Normalized		
SBA-15 (6 nm)	0	0	1.11	1	842	1	–
Mo(4)/SBA-15 (6 nm)	3.5	0	0.79	0.75	549	0.70	3.1
Mo(9)/SBA-15 (6 nm)	9.1	0	0.70	0.74	505	0.71	3.6
Mo(16)/SBA-15 (6 nm)	16.3	0	0.58	0.70	388	0.63	3.8
Co(2)Mo(7)/SBA-15 (6 nm)	6.7	1.7	0.63	0.66	474	0.64	3.5
Co(2)Mo(10)/SBA-15 (6 nm)	10.4	1.9	0.53	0.62	363	0.55	3.1
Co(3)Mo(14)/SBA-15 (6 nm)	14.4	2.8	0.52	0.65	396	0.64	6.7
Co(2)Mo(20)/SBA-15 (6 nm)	19.6	1.7	0.39	0.57	299	0.58	4.0
SBA-15 (9 nm)	0	0	1.13	1	467	1	–
Mo(11)/SBA-15 (9 nm)	11.2	0	0.86	0.93	376	0.98	3.4
Co(2)Mo(11)/SBA-15 (9 nm)	11.1	2.0	0.81	0.97	350	0.96	3.9
Co(2)Mo(20)/SBA-15 (9 nm)	20.0	1.7	0.58	0.88	263	0.92	5.1

Normalized(X) = $X_{(Co)\text{-}Mo}/((1-y)\ X_{SBA\text{-}15})$, where X is specific surface area (pore volume), y is weight fraction of (Co)Mo sulfides

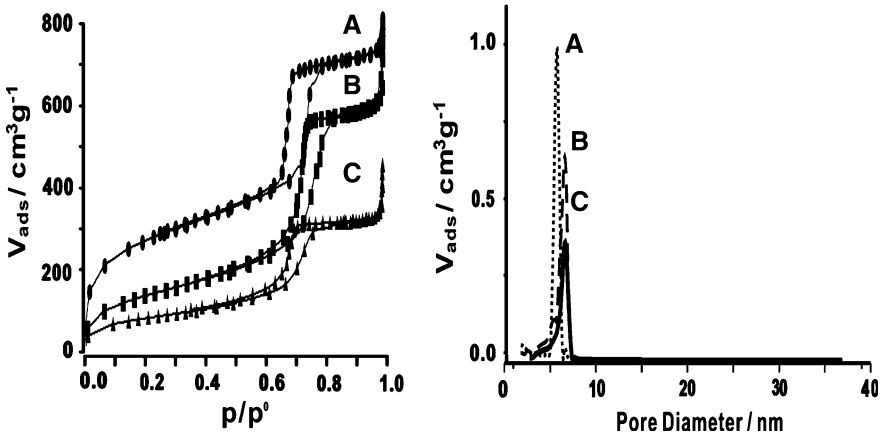

Fig. 3 Nitrogen adsorption/desorption isotherms (*left*) and BJH pore-size distribution (*right*). (A) SBA-15 (6 nm); (B) Mo(9)/SBA-15 (6 nm) and (C) Co(2)Mo(20)/SBA-15 (6 nm)

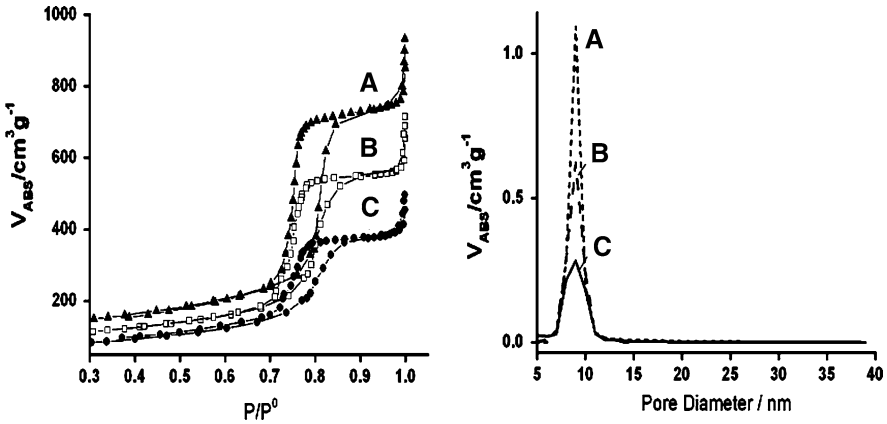

Fig. 4 Nitrogen adsorption/desorption isotherms (*left*) and BJH pore-size distribution (*right*). (A) SBA-15 (9 nm); (B) Mo(11)/SBA-15 (9 nm) and (C) Co(2)Mo(20)/SBA-15 (9 nm)

3.3 Transmission Electron Microscopy

All particles exhibit a well ordered arrangement of cylindrical mesopores as expected for filled SBA-15. The perfection of the mesoporous structure along the channels axes is exemplified in the bright-field image of Fig. 5a. The hexagonal arrangement of the spots indicates the periodicity which is also supported by the attached Fourier

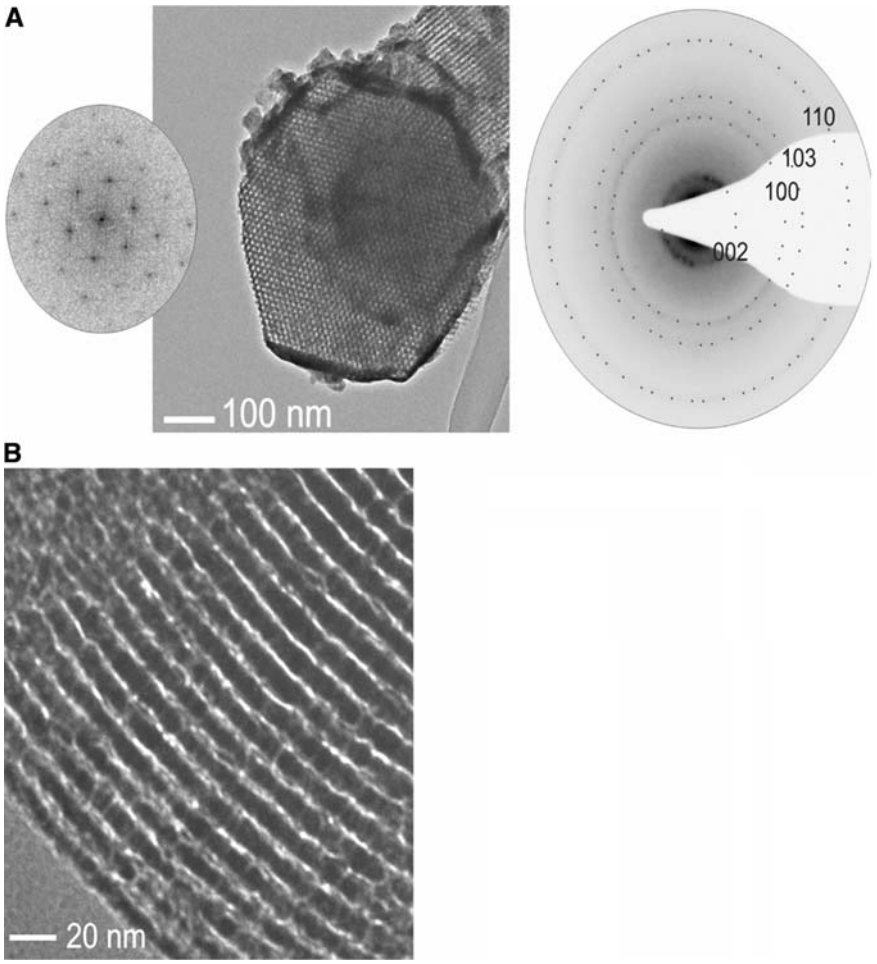

Fig. 5 Bright field images of Co-Mo/SBA-15 (9 nm): (**a**) Recorded along the channels axis with FFT (left, calculated on a square section) and SAED pattern (right, the *d*-values match MoS_2); and (**b**) recorded perpendicular to the channels axis

transform (FFT in Fig. 5a, left). The latter exhibits sharp peaks with significant intensity even for the higher order signals. The *d*-spacing of ca. 10.4 Å matches an average value of d_{100} determined on different particles and in distinct orientations. EDX spectra contain separated peaks for the metals, namely Co- and Mo-K, but coinciding peaks for Mo and S (Mo-L and S-K). Therefore, only the presence of Mo and Co can unambiguously be analyzed. The ratio of Mo:Co varies significantly in different particles. SAED patterns display faint diffuse intensities located on concentric rings around 000. The *d*-values are close to those expected for MoS_2 (see brackets, [29]): $d_{002} = 6.2$ (6.15) Å, $d_{100} = 2.80$ (2.74) Å, $d_{103} = 2.31$ (2.28) Å, $d_{110} = 1.60$ (1.58) Å) supporting the presence of randomly oriented and nanosized $CoMoS_2$ crystals.

In some areas the diffuse intensity is resolved into broad reflections indicating larger $CoMoS_2$ crystals which were found to adhere to the surface of the mesoporous host. To check whether the metal containing components are also located inside the pores wide angle tilting and EDX were combined. The particle of Fig. 5b was not covered with Co promoted MoS_2 crystals on the surface as shown by wide angle tilting, however EDX spectra indicate the presence of Mo and Co, respectively. When aligning the particle perpendicular to the channels axis, the interior of the parallel channels display a random arrangement of dark spots suggesting the presence of $CoMoS_2$-nanoparticles inside the host.

In an independent approach in situ transformation was applied to demonstrate the filling of the mesoporous host. The particle of Fig. 5a was irradiated under massive exposure conditions by removing the condenser aperture (increase of the beam current by a factor of 40). The mesoporous structure collapses immediately and releases many $CoMoS_2$-nanoparticles onto the surface of the host as evidenced by EDX and SAED, see Fig. 6a. HRTEM micrographs performed on single $CoMoS_2$-nanoparticles show the layered structure of the MoS_2-type, see Fig. 6b. The FFT of a square region of Fig. 6b indicates a layer spacing close to 6.2 Å which corresponds with d_{002}. Such experiments were repeated several times on distinct particles, giving clear evidence for the presence of Co promoted MoS_2 inside the channels of SBA-15. MoS_2 crystallites with average length of 15 nm and average stacking of

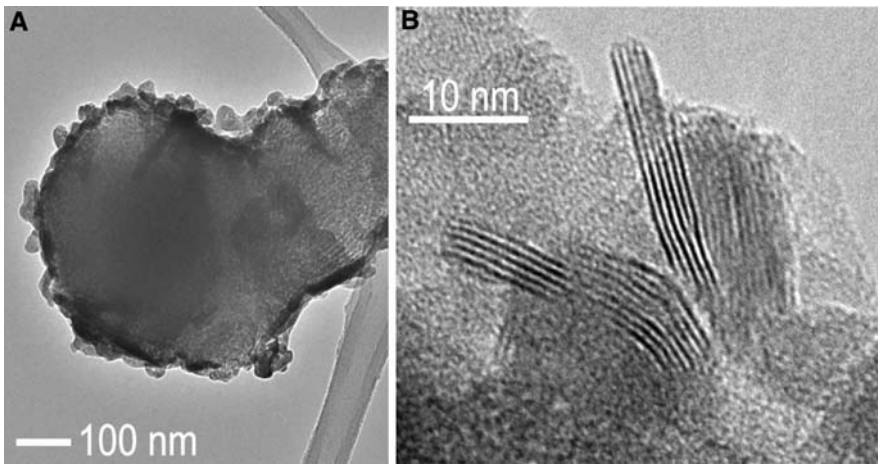

Fig. 6 (**a**) Particle of Fig. 5a after in situ transformation and (**b**) HRTEM micrograph of MoS_2 particles promoted with Co nanocrystals

about 6 layers (~4 nm, in good agreement with the XRD measurements) are observed (Fig. 6b), which are obviously larger than the SBA-15 supported MoS_2 catalysts synthesized from the oxide precursors (length = 2–6 nm, average stacking = 3.5 [11].) The thermal decomposition of ATM on SBA-15 leads to a relatively poor MoS_2 dispersion which may be attributed to the weak interaction between the sulfides and the SBA-15 support with a low number of Si-OH groups and a low acidity.

3.4 Catalytic HDS Activity and Selectivity

The HDS of DBT can occur by two reactions pathways: (I) direct desulfurization (DDS) via C–S bond cleavage leading to the formation of biphenyl (BP), and (II) hydrogenation (HYD) to form phenylcyclohexane (PCH), which is a secondary product yielded from the desulfurization of tetrahydrodibenzothiophene (TH-DBT) and hexahydrodibenzothiophene (HH-DBT). For Ni(Co)-MoS_2 catalysts only TH-DBT can be observed [30]. Therefore, the catalytic selectivity determined from the ratio between HYD and DDS can be approximated by the following equation:

$$S_{HYD}/S_{DDS} = ([PCH] + [TH - DBT])/[BP]$$

In the present study, the catalytic activity of MoS_2/SBA-15 and Co-MoS2/SBA-15 catalysts was examined in the HDS of DBT. Several effects can be observed analyzing the measurement results carefully.

Figure 7 illustrates the dependency of DBT conversion and catalytic selectivity as function of Mo loading and pore diameter of SBA-15 for MoS_2/SBA-15 catalysts. For the catalysts supported on 6 nm SBA-15, the increasing catalytic activity is accompanied by a significant increase of the yields of hydrogenation products such as PCH and TH-DBT.

According to the study of Prins et al. [30] the two HDS pathways are determined by the orientation of the adsorbed DBT molecules with respect to the catalysts surface. The DDS pathway occurs through σ adsorption via the sulfur atom and HYD through π adsorption via the aromatic system. The π adsorption is a flat adsorption of the molecules covering a large part of the catalyst surface. Therefore, hydrogenation of DBT should be a sterical demanding reaction pathway. To explain the catalytic selectivity during HDS the rim-edge model was presented by Daage and Chiannelli [31]. The model proposes that hydrogenation of DBT occurs exclusively on rim sites, whereas direct HDS occurs on both rim and edges sites. Assuming this model, the increase of HYD products of the MoS_2/SBA-15 catalysts may be probably caused by the development of a larger amount of rim sites in the active phase. But it should be emphasized that the rim-edge model was proposed for unsupported MoS_2 catalysts. An increasing amount of MoS_2 slabs with increasing Mo loading might be located on the external surface of SBA-15. Therefore, with increasing Mo loading more hydrogenation products can be obtained from the reaction occurring on these externally located MoS_2 slabs because there is no sterical hindering. But one should keep in mind that the external surface area is much smaller compared to the internal surface area.

A confinement effect [17] is obvious comparing MoS_2 catalysts supported on 6 nm and 9 nm SBA-15: a significant enhancement of the hydrogenation reactivity is observed for MoS_2 supported on SBA-15 with the larger diameter of about 9 nm ($S_{HYD}/S_{DDS} = 1.57$, 11 wt.% Mo, see Fig. 7), despite the lower Mo loading compared to the catalyst supported on 6 nm material (16 wt.% Mo; $S_{HYD}/S_{DDS} = 1.43$). This finding highly suggests that the mesoporous channels of the support are responsible for this effect. The channel diameter of SBA-15 may hinder the sterically demanding π adsorption of DBT molecules and

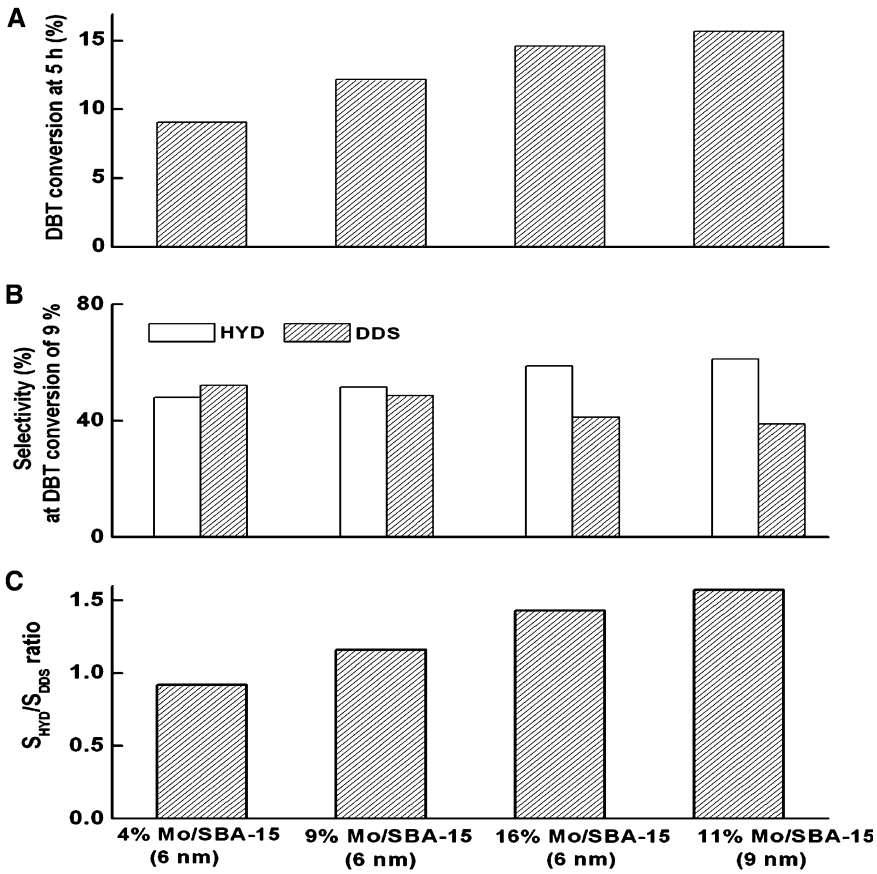

Fig. 7 HDS of DBT over MoS_2/SBA-15 at $T = 623$ K, $P = 3.4$ MPa: (**a**) total DBT conversion at 5 h of reaction time; (**b**) selectivties achieved at a DBT conversion of ca. 9% (different reaction times); (**c**) S_{HYD}/S_{DDS} selectivity ratio achieved at DBT conversion of ca. 9% (different reaction times).

induces the lower S_{HYD}/S_{DDS} ratio for 6 nm SBA-15 which shows in addition a significant pore blocking (see the results of nitrogen physisorption measurements).

Figure 8 shows the HDS performance and the selectivity of Co-MoS_2/SBA-15 catalysts and the two references taken from [13]. It is obvious that the incorporation of Co yields significantly higher conversions of DBT (4–6 times) compared to the unpromoted MoS_2/SBA-15 catalysts. The catalytic activities of Co-MoS_2/SBA-15 show a systematic increase with increasing Mo content. Moreover, MoS_2/SBA-15 promoted with Co at Mo loadings up ca. 10 wt.% displays also a higher catalytic activity (ca. 62–93% DBT conversion after 5 h) compared with Co-MoS_2/SBA-15 prepared by the oxide precursors (10 wt.% Mo loading, ca. 54% DBT conversion [14]) as well as the commercial CoMo/γ-Al_2O_3 (ca. 53% DBT conversion [14]), despite the presence of the pronounced stacking of MoS_2 slabs and the low Co content (ca. 2%). The enhancement of the catalytic activity is mainly due to the preference for the DDS pathway during the desulfurization of DBT (Fig. 8).

The high HDS activity suggests that MoS_2 stacking is not a prerequisite for a good performance and also not a sign of deactivation or lower activity. This suggestion is in agreement with the study of Eijsbouts et al. [32]. In this study the catalytic activity of unsupported liquid-phase-sulfided Type 2 commercial ULSD catalysts was compared with respect to the size, shape and stacking of MoS_2. The main result of the investigations is that the synthesis procedure determines the activity of a catalyst. From the occurrence or absence of MoS_2 stacking one cannot conclude whether a catalyst is more or less active. But such a systematic study of supported HDS catalysts was not performed until now.

It is well known that a high HDS performance of the catalysts is connected with the presence of the so-called CoMoS phase with Co atoms being located at the edges of the layered MoS_2 structure [33]. In our experiments the cobalt sulfide is formed first and part of Co species may migrate to the edges of MoS_2 yielding the catalytic active CoMoS phase during the thermal decomposition of ATM. The XRD measurements indicate an increasing formation of CoMoS phase with increasing Mo loading. Moreover, segregated Co_9S_8 (Fig. 2) may play a distinct catalytic role according to the "Remote Control" concept [34]: hydrogen is dissociated to spill-over hydrogen H_{SO} on Co_9S_8; it migrates to the surface of MoS_2 or CoMoS phases. In addition, "vacancies" or coordinatively unsaturated sites ("CUS") which are created by the reaction of hydrogen with surface sulfide groups during the thermal treatment of the ATM precursor in a H_2/N_2 atmosphere may be

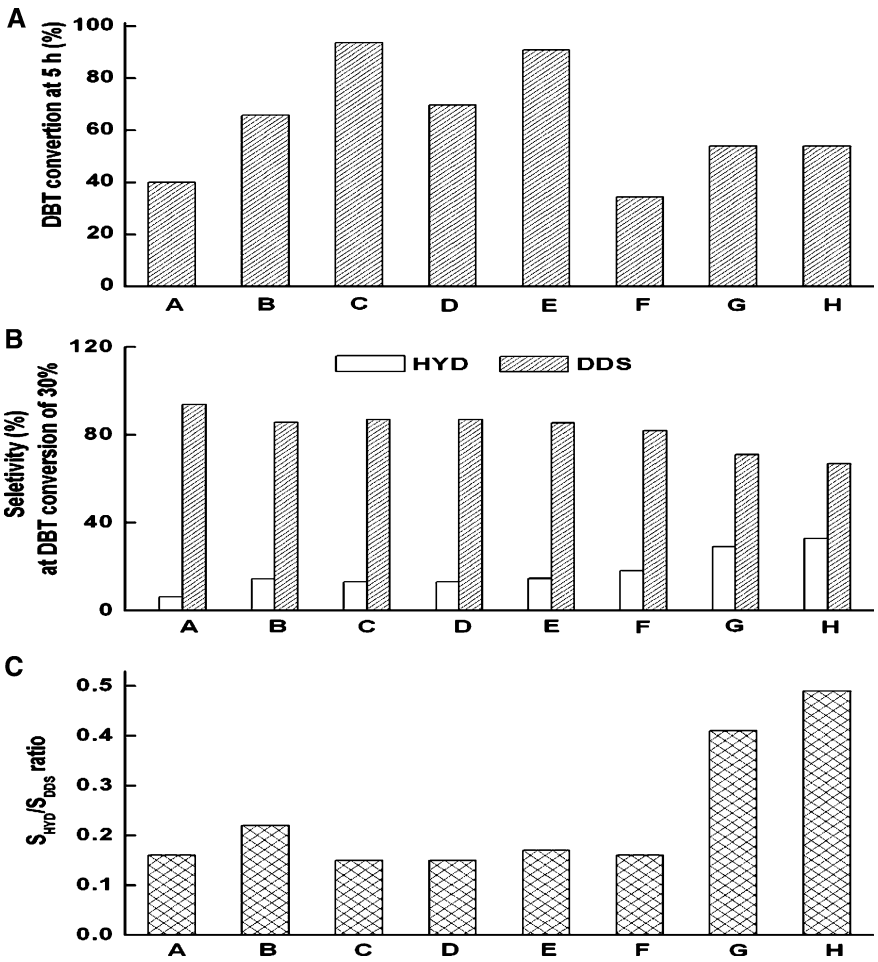

Fig. 8 HDS of DBT over Co-Mo/SBA-15 at $T = 623$ K, $P = 3.4$ MPa: (**a**) Total DBT conversion at 5 h of reaction time; (**b**) Selectivties achieved at a DBT conversion of ca. 30% (different reaction times); (**c**) S_{HYD}/S_{DDS} selectivity ratio achieved at DBT conversion of ca. 30% (different reaction times), for the samples A: Co(2)Mo(7)/SBA-15 (6 nm); B: Co(2)Mo(10)/ SBA-15 (6 nm); C: Co(2)Mo(20)/SBA-15 (6 nm); D: Co(2)Mo(10)/ SBA-15 (9 nm); E: Co(2)Mo(20)/SBA-15 (9 nm); F: Co(3)Mo(14)/ SBA-15 (6 nm), G: Co(3)Mo(10)/SBA-15 (reported by [13]); and H: $CoMo/Al_2O_3$ [13]

responsible for high activity of the catalysts. In view of the results of the HRTEM study (poor dispersion of MoS_2 phase) it is most likely that the CUS mainly contribute to the unexpected high catalytic activity.

The selectivity expressed as the S_{HYD}/S_{DDS} ratios for our Co-MoS_2/SBA-15 catalysts ($\sim$0.20) is apparently higher compared to the unpromoted MoS_2/SBA-15 and the commercial CoMo/γ-Al_2O_3 catalysts ($\sim$0.49) (Fig. 8), i.e., the Co promoted catalysts show a much lower HYD than DDS in agreement with observations made previously [35]. The significant increase of the selectivity going from pure MoS_2 to Co promoted catalysts is a strong evidence for the generation of the active CoMoS phases. Another factor for the high selectivity may be the special features of the mesoporous SBA-15 support as shown for the unpromoted MoS_2/SBA-15 catalysts. It seems that the mesopores of SBA-15 hinder the flat DBT adsorption through the adsorption of π electrons of DBT (HYD pathway) and favor the direct C–S bond cleavage (DDS pathway) leading to an enhancement of the selectivity (confinement effect). A similar observation was made by Fierro and co-workers where Co-MoS_2/SBA-15 catalysts showed a slightly higher selectivity ($S_{HYD}/S_{DDS} \sim 0.4$) compared to a CoMo/γ-Al_2O_3 catalyst ($\sim$0.49) despite that both materials have been prepared via the same route [14]. However, no changes of the selectivity are observed by increasing the Mo loading. In addition, the enlargement of the pore size of SBA-15 from 6 nm to 9 nm (Fig. 8) has also no effect onto the selectivity. Obviously, the confinement effect due to the mesopore channels is here not the dominating effect. An interesting finding is that our catalysts have a clearly higher selectivity ($\sim$0.2 vs. $\sim$0.4) compared to the Co-MoS_2/SBA-15 catalysts prepared by Fierro and co-workers despite the same support material (SBA-15) (Fig. 8). A large number of studies suggest that the hydrogenolysis and hydrogenation reactions occur on separate sites, Lewis acid sites (vacancies) and Brønsted acid sites, respectively [14]. The absence of Brønsted acid sites of the SBA-15 support has been confirmed by means of FTIR spectroscopy [14]. Therefore, the pronounced selectivity for the DDS route could be related to the presence of a large amount of CUS (Lewis acid sites) in our catalysts, which were formed during the thermal treatment of the ATM material under H_2/N_2 atmosphere. Moreover, the hydrogenation of DBT is a steric demanding reaction and the decrease of HYD production may indicate an inhibition of

the flat DBT adsorption on the active sites. Applying the rim-edge model proposed by Daage and Chianelli, the lower HYD activity observed for our catalysts compared to the Co-MoS_2/SBA-15 catalysts prepared by Fierro and co-workers may be due a smaller amount of rim sites in the catalytic active phases.

Based on simple considerations one would expect that 9 nm SBA-15 supported catalysts with a negligible pore blocking should have a significantly higher HDS activity compared with the 6 nm SBA-15 support (larger pore blocking). However, Co-MoS_2/SBA-15 (6 nm) exhibits the highest catalytic activity (Fig. 8) due to the larger specific surface area with respect to 9 nm SBA-15. The optimal atomic Co/Mo ratio of 0.4 was found for γ-Al_2O_3 supported HDS catalysts [36]. Consequently, the cobalt loading was increased in the SBA-15 supported catalysts as an attempt to increase the HDS activity. But the relative high Co loading of about 3 wt.% leads to lower catalytic activity (Fig. 8f) which may be due to the formation of a smaller amount of the active CoMoS phases. Eventually, the higher Co concentration causes a partial pore blocking of the SBA-15 channels thus hindering the dispersion of ATM along the channel walls leading to a poor dispersion of MoS_2 particles (Table 1).

4 Conclusions

We have demonstrated that catalytically active MoS_2 and MoS_2 promoted with Co phases located inside of the pores of the support SBA-15 (HRTEM) can be prepared by thermal decomposition of suitable thiosalt precursors. Despite the large MoS_2 stacking and the presence of long slabs (HRTEM, XRD) the catalysts show a higher HDS activity compared to a commercial CoMo/γ-Al_2O_3 catalyst. This observation suggests that a good performance for the HDS reaction is not simply related to these structural features of the catalytically active material. An explanation for the observed high HDS activity bases on the co-operative or synergistic effect of a CoMoS phase, Co_9S_8 as well as a large amount of vacancies (CUS). The latter are introduced during the thermal treatment of the ATM precursor in a reducing atmosphere. Hence, the present results are another example that the synthetic route plays an important role for the preparation of active catalysts. For unpromoted MoS_2/SBA-15 catalysts a confinement effect caused by the different sizes of the mesoporous channels is observed. SBA-15 support with the larger channel diameter of 9 nm and a Mo loading of 11 wt.% has a higher activity for the HYD pathway compared to SBA-15 with 6 nm channel diameter and 16 wt.% Mo loading. This result demonstrates the importance of the support for the catalytic activity which was recently discussed in detail [37, 38]. For the catalysts promoted with Co supported on SBA-15 the confinement effect seems to be less pronounced. Co-MoS_2/SBA-15 (6 nm) exhibits the highest catalytic activity despite the more significant pore blocking compared to Co-MoS_2/SBA-15 (9 nm) (nitrogen physisorption experiments). This observation may be attributed to the larger surface area of the SBA-15 support with the smaller pore size of 6 nm. In total, the results demonstrate that Co-Mo sulfide catalysts using ATM as precursor supported on SBA-15 are good candidates for the conversion of DBT and petroleum residues. Further studies are under way to explore different synthesis routes for the preparation of more active catalysts using SBA-15 as support material.

Acknowledgment The financial support of the Deutsche Forschungsgemeinschaft (DFG) and of the State of Schleswig-Holstein is greatly acknowledged.

References

1. Beck JS, Vartuli JC, Roth WJ, Leonowicz ME, Kresge CT, Schmitt KD, Chu CT-W, Olson DH, Sheppard EW, McCullen SB, Higgins JB, Schlenker JL (1992) J Am Chem Soc 114:10834
2. Kresge CT, Leonowicz ME, Roth WJ, Vartuli JC, Beck JS (1992) Nature 359:710
3. Zhao D, Feng J, Huo Q, Melosh N, Fredrickson GH, Chmelka BF, Stucky GD (1998) Science 279:548
4. Song CS, Reddy KM (1999) Appl Catal A – Gen 176:1
5. Wang AJ, Wang Y, Kabe T, Chen YY, Ishihara A, Qian WH (2001) J Catal 199:19
6. Wang AJ, Wang Y, Kabe T, Chen YY, Ishihara A, Qian WH, Yao PJ (2002) J Catal 210:319
7. Sampieri A, Pronier S, Blanchard J, Breysse M, Brunet S, Fajerwerg K, Louis C, Pérot G (2005) Catal Today 107–108:537
8. Vradman L, Landau MV, Herskowitz M, Ezersky V, Talianker M, Nikitenko S, Koltypin Y, Gedanken A (2003) J Catal 213:163
9. Vradman L, Landau MV, Herskowitz M, Ezersky V, Talianker M, Nikitenko S, Koltypin Y, Gedanken A (2003) Stud Surf Sci Catal 146:721
10. Dhar GM, Kumaran GM, Kumar M, Rawat KS, Sharma LD, Raju BD, Rao KSR (2005) Catal Today 99:309
11. Gutiérrez OY, Fuentes GA, Salcedo C, Klimova T (2006) Catal Today 116:485
12. Gutiérrez OY, Valencia D, Fuentes GA, Klimova T (2007) J Catal 249:138
13. Kumaran GM, Garg S, Soni K, Kumar M, Sharma LD, Dhar GM, Rao KSR (2006) Appl Catal A – Gen 305:123
14. Nava R, Ortega RA, Alonso G, Ornelas C, Pawelec B, Fierro JLG (2007) Catal Today 127:70
15. Coulier L, Kishan G, van Veen JAR, Niemantsverdriet JW (2002) J Phys Chem B 106:5897
16. Alonso G, Del Valle M, Cruz J, Petranovskii V, Licea-Claverie A, Fuentes S (1998) Catal Today 43:117
17. Alonso G, Berhault G, Aguilar A, Collins V, Ornelas C, Fuentes S, Chianelli RR (2002) J Catal 208:359
18. Nava H, Ornelas C, Aguilar A, Berhault G, Fuentes S, Alonso G (2003) Catal Lett 86:257
19. Huirache-Acuña R, Albiter MA, Ornelas C, Paraguay-Delgado F, Martínez-Sánchez R, Alonso-Nuñez G (2006) Appl Catal A – Gen 308:134

20. Brito JL, Severino F, Delgado NN, Laine J (1998) Appl Catal A – Gen 173:193
21. Rivera-Muños ER, Lardizabal D, Alonso G, Aguilar A, Siadati MH, Chianelli RR (2003) Catal Lett 85:147
22. Brieler FJ, Fröba M, Chen LM, Klar PJ, Heimbrodt W, von Nidda HAK, Loidl A (2002) Chem Eur J 8:185
23. Brieler FJ, Grundmann P, Fröba M, Chen LM, Klar PJ, Heimbrodt W, von Nidda HAK, Kurz T, Loidl A (2004) J Am Chem Soc 126:797
24. Huang Z-D, Bensch W, Sigle W, van Aken PA, Kienle L, Vitoya T, Modrow H, Ressler T (2007) J Mater Sci in press
25. Barrett EP, Joyner LG, Halenda PP (1951) J Am Chem Soc 73:373
26. Thommes M, Köhn R, Fröba M (2000) J Phys Chem B 104:7932
27. Thommes M, Köhn R, Fröba M (2002) Appl Surf Sci 196:239
28. Appendix to IUPAC Manual of symbols and terminology, Part 1 (1972) Pure Appl Chem 31:579
29. Bronsema KD, de Boer JL, Jellinek F (1986) Z Anorg Allg Chem 540:15
30. Prins R, Egorova A, Rothlisberger A, Zhao Y, Sivasankar N, Kukula P (2006) Catal Today 111:84
31. Daage M, Chianelli RR (1994) J Catal 149:414
32. Eijsbouts S, van den Oetelaar LCA, van Puijenbroek RR (2005) J Catal 229:352
33. Topsøe H, Clausen BS (1984) Catal Rev – Sci Eng 26:395
34. Karroua M, Matralis H, Grange P, Delmon B (1993) J Catal 139:371
35. Bataille F, Lemberton J-L, Michaud P, Pérot G, Vrinat M, Lemaire M, Schulz E, Breysse M, Kasztelan S (2000) J Catal 191:409
36. Al-Zeghayer YS, Sunderland P, Al-Masry W, Al-Mubaddel F, Ibrahim AA, Bhartiya BK, Jibril BY (2005) Appl Catal A – Gen 282:163
37. Dhar GM, Srinivas BN, Rana MS, Kumar M, Maity SK (2003) Catal Today 86:45
38. Breysse M, Afanasiev P, Geantet C, Vrinat M (2003) Catal Today 86:5